BIOCHEMISTRY
including biophysical chemistry & molecular biology

Article

pubs.acs.org/biochemistry

Two Parallel Pathways in the Kinetic Sequence of the Dihydrofolate Reductase from *Mycobacterium tuberculosis*

Clarissa M. Czekster,* An Vandemeulebroucke,* and John S. Blanchard

Department of Biochemistry, Albert Einstein College of Medicine, 1300 Morris Park Avenue, Bronx, New York 10461, United States

Supporting Information

ABSTRACT: Dihydrofolate reductase from *Mycobacterium tuberculosis* (*Mt*DHFR) catalyzes the NAD(P)H-dependent reduction of dihydrofolate, yielding $NAD(P)^+$ and tetrahydrofolate, the primary one-carbon unit carrier in biology. Tetrahydrofolate needs to be recycled so that reactions involved in dTMP synthesis and purine metabolism can be maintained. Previously, steady-state studies revealed that the chemical step significantly contributes to the steady-state turnover number, but that a step after the chemical step was likely limiting the reaction rate. Here, we report the first pre-steady-state investigation of the kinetic sequence of the *Mt*DHFR aiming to identify kinetic intermediates, and the identity of the rate-limiting steps. This kinetic analysis suggests a kinetic sequence comprising two parallel pathways with a rate-determining product release. Although product release is likely occurring in a random fashion, there is a slight preference for the release of THF first, a kinetic sequence never observed for a wild-type dihydrofolate reductase of any organism studied to date. Temperature studies were conducted to determine the magnitude of the energetic barrier posed by the chemical step, and the pH dependence of the chemical step was studied, demonstrating an acidic shift from the pK_a observed at the steady state. The rate constants obtained here were combined with the activation energy for the chemical step to compare energy profiles for each kinetic sequence. The two parallel pathways are discussed, as well as their implications for the catalytic cycle of this enzyme.

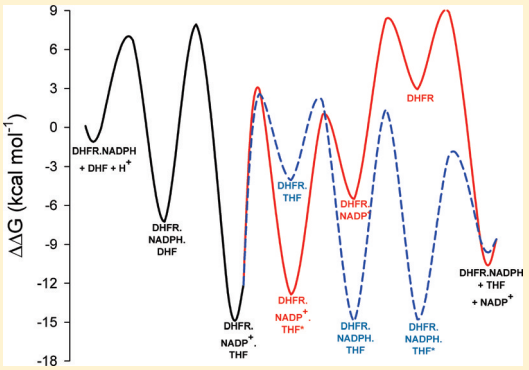

Dihydrofolate reductase (5,6,7,8-tetrahydrofolate:$NADP^+$ oxidoreductase, EC 1.5.1.3, DHFR) catalyzes the NADPH-dependent reduction of dihydrofolate (DHF) to tetrahydrofolate (THF) (Scheme 1). This enzyme is required for the regeneration of THF, a crucial one-carbon unit carrier essential for reactions involved in deoxythymidine monophosphate (dTMP) synthesis, as well as reactions involved in the biosynthesis of purines.[1] Drugs that inhibit DHFR have been used since 1947, when aminopterin was introduced in the treatment of leukemia,[2] followed by the development of pyrimethamine and trimethoprim in the 1950s, which were found to be effective in the treatment of malaria and bacterial infections.[3] In addition to their relevance as a drug target, DHFRs from several organisms have been thoroughly studied kinetically and structurally, improving our understanding of protein folding,[4] the importance of dynamics and coupled motions to catalysis,[5] and the contribution of chemistry and conformational changes to catalysis,[6] just to name a few. Recently, our group demonstrated by a combination of pH studies and kinetic isotope effects under steady-state and pre-steady-state conditions that the chemical step of the DHFR from *Mycobacterium tuberculosis* (*Mt*DHFR) had a remarkably slow rate at neutral pH compared to the rates of DHFRs from other organisms.[7] Additionally, it was demonstrated that the chemical step was contributing significantly to the turnover rate of the reaction, but that a step after the chemical step was decreasing the magnitude of the kinetic isotope effects observed under steady-state conditions. In this work, we investigate the kinetic sequence of *Mt*DHFR by stopped-flow absorbance and fluorescence, aiming to identify which step is the rate-determining step in turnover and whether this reaction follows a preferential pathway, as seen for other DHFRs.[8−14] Our kinetic analysis allowed us to put forward a complex kinetic sequence based on a slow chemical step followed by rate-limiting random product release occurring via two possible, and likely parallel, pathways.

EXPERIMENTAL PROCEDURES

Materials. All chemicals were of analytical or reagent grade and were used without further purification. DHF, THF, NADPH, and $NADP^+$ were purchased from Sigma.

Purification of *Mt*DHFR. Competent *Escherichia coli* BL21(DE3) cells (Novagen) were transformed with recombinant plasmid pET28a(+):*dfrA*, and *Mt*DHFR was expressed and purified as described previously.[15] Protein concentrations were determined by using the theoretical value of 40450 M^{-1} cm^{-1} for ε_{280} or 6220 M^{-1} cm^{-1} for ε_{340} due to bound NADPH.[16] The $NADP^+$-bound form of the enzyme was generated by immobilizing *Mt*DHFR-NADPH onto a Ni-NTA resin, and

Received: April 20, 2011
Revised: July 8, 2011
Published: July 11, 2011

Scheme 1. Reaction Catalyzed by *Mt*DHFR

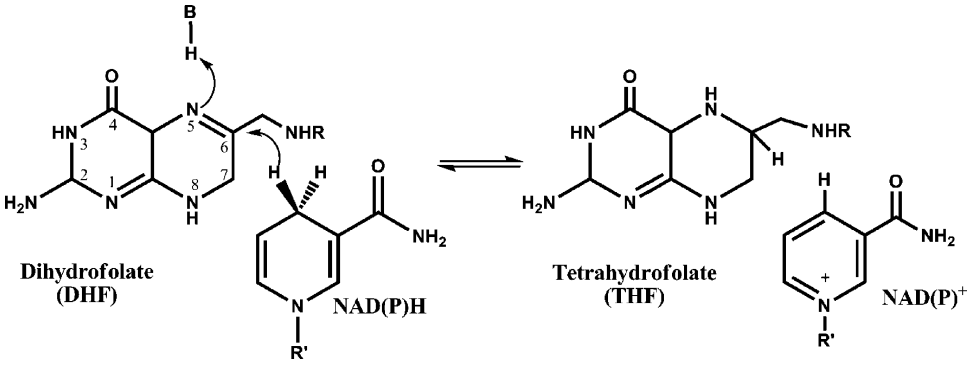

10 mL of 100 mM $NADP^+$ was passed through the column, yielding the *Mt*DHFR-$NADP^+$ form of the enzyme. The enzyme was eluted with 500 mM imidazole, dialyzed against 2 × 2 L of 100 mM HEPES with 50 mM KCl (pH 7.5), and frozen at −80 °C.

Equilibrium Dissociation Constants. Binding of THF to *Mt*DHFR-NADPH and *Mt*DHFR-$NADP^+$ was measured by fluorescence titration at 25 °C using a Horiba spectrofluorometer. Excitation and emission wavelengths were 280 and 340 nm, respectively. Titrations were conducted by serial additions of 1 μL aliquots of ligand to a 1 cm^2 quartz cuvette that contained 2 mL of 0.5 μM *Mt*DHFR in 100 mM HEPES with 50 mM KCl (pH 7.5). Fluorescence readings were recorded 2 min after the addition of ligand to allow temperature equilibration, and the dissociation constants were estimated by nonlinear regression. Data for binding of THF to *Mt*DHFR-NADPH were fitted to a quadratic equation (eq 1) due to the fact that the concentration of enzyme and ligand were comparable, whereas data for binding of THF to *Mt*DHFR-$NADP^+$ were fitted to a hyperbolic equation (eq 2)

$$F = \frac{E_0 + S_T + K_d - \sqrt{(E_0 + S_T + K_d)^2 - 4E_0S_T}}{2E_0} \quad (1)$$

$$F = \frac{S}{K_d + S} \quad (2)$$

where F is the fraction of ligand bound to the enzyme, E_0 is the initial enzyme concentration, S_T is the total ligand concentration, S is the substrate concentration, and K_d is the dissociation constant for the enzyme−substrate complex.[17]

The concentration of THF did not exceed 10 μM to avoid inner filter effects.

Stopped-Flow General Procedures. All pre-steady-state experiments were performed on an Applied Photophysics model SX20 stopped-flow spectrofluorometer equipped with a xenon lamp, which has a dead time of 3 ms, and a 1 cm path length for absorbance measurements and a 2 mm path length for fluorescence measurements. All experiments were performed at 25 °C in 100 mM HEPES and 50 mM potassium chloride buffer (pH 7.5), unless stated otherwise. Typically, each observed rate constant was obtained after averaging 5−10 shots, and fitting the average to the appropriate exponential equation. The reported concentrations are final, after volumes of 60 μL were mixed from each syringe.

Stopped-Flow Absorption Experiments. The conversion of DHF and NADPH to THF and $NADP^+$ was monitored by observing the change in absorbance at 340 nm, using an extinction coefficient of 11800 M^{-1} cm^{-1}.[18] For single-turnover experiments, the DHF concentration was kept at 1 μM and the NADPH concentration was saturating (100 μM), while the concentration of *Mt*DHFR was varied from 5 to 28 μM. Traces were fitted analytically using Microsoft Origin version 7, and the first 3 ms of data was discarded when the data were fit. Inspection of residuals provided an assessment of the quality of the fits. The fitting functions had a general form (eq 3)

$$y(t) = \sum_i A_i e^{-k_i t} + C \quad (3)$$

where $y(t)$ is the observed signal at time t, i is the number of transients, A_i is the amplitude of the ith transient, k_i is the observed rate constant for the ith transient, and C is the offset.

Multiple turnovers were measured by monitoring the change in absorbance at 340 nm. For these experiments, the concentrations of DHF and NADPH were 100 μM each, and the *Mt*DHFR concentration was varied from 1 to 10 μM. The curves obtained were fitted to eq 4, which is identical to eq 3 but includes a linear phase, whose rate is represented by v.

$$y(t) = \sum_i A_i e^{-k_i t} + vt + C \quad (4)$$

Stopped-Flow Fluorescence Experiments. Single and multiple turnovers were also monitored by using fluorescence energy transfer (FRET), emitted when the protein is excited at 280 nm, emitting fluorescence at 340 nm, which then excites the bound NADPH molecules, emitting fluorescence at 450 nm. A cutoff filter of 420 nm was used to ensure that only the signal coming from the transfer was being observed. The conditions were the same as those described for the stopped-flow absorbance measurements. Binding and dissociation rate constants were measured by stopped-flow fluorescence quenching or enhancement, and the measurement of dissociation rates utilized NADPH, $NADP^+$, or methotrexate as a competitor. For binding experiments monitoring protein fluorescence, the concentration of THF did not exceed 10 μM to avoid inner filter effects. THF binding experiments were also conducted using FRET, which significantly decreases inner filter effects. Binding of DHF to *Mt*DHFR-NADPH was measured by performing single-turnover experiments with 2 μM DHF, 100 μM NADPH, and variable concentrations of enzyme (at least 5 times higher than the concentration of DHF, to maintain pseudo-first-order conditions). Observed rate constants obtained after fitting the data to eq 1 were used in replots of k_{obs} versus concentrations of substrate, product, or competitor. Linear

dx.doi.org/10.1021/bi200608n | *Biochemistry* 2011, 50, 7045−7056

concentration dependencies of the observed rate constant (k_{obs}) were fitted to eq 5

$$k_{obs1} = k_1[L] + k_{-1} \quad (5)$$

where k_1 is the association rate constant, L is the concentration of ligand, and k_{-1} is the dissociation rate constant. When binding was a two-step process, data for the first phase were fitted to a modified version of eq 5, in which the intercept is equal to $k_1 + k_2 + k_{-2}$.[19]

Hyperbolic concentration dependencies of the observed rate constant (k_{obs2}) were fitted to eq 6. Hyperbolic concentration dependency refers to a two-step binding process.

$$k_{obs2} = \frac{k_1[L](k_{-2} + k_2) + k_{-1}k_{-2}}{k_1[L] + k_{-1} + k_2 + k_{-2}} \quad (6)$$

The apparent dissociation constant (K_{ov}) for this two-step association was obtained using eq 7.

$$K_{ov} = \frac{k_{-1}k_{-2}}{k_1(k_2 + k_{-2})} \quad (7)$$

When saturation of the second phase (k_{obs2}) was not observed, and the concentration of the ligand could not be increased because of inner filter effects, data were fitted to the following linear equation (eq 8), a simplification of eq 6 for $[L] \ll K_s$

$$k_{obs2} = (k_2/K_s)[L] + k_{-2} \quad (8)$$

In eqs 6−8, k_1 is the association rate constant, k_{-1} is the dissociation rate constant, k_2 and k_{-2} are the forward and reverse rate constants, respectively, of the unimolecular isomerization step, and K_s is the dissociation constant for the first bimolecular step. Equations for pre-steady-state analysis were adapted from ref 20.

Temperature and pH Dependence of the Chemical Step. Single-turnover experiments were conducted at 15−35 °C. The rate constants for the chemical step (k_H) obtained after fitting the single-turnover transients with a single-exponential equation (eq 4) were replotted as a function of temperature, and the activation energy was calculated from fitting the temperature dependence of k_H to eq 9. The temperature dependence of k_{cat} data was also fitted to eq 9.

$$\ln(k) = (E_a/R)(1/T) + \ln(A) \quad (9)$$

Additionally, rate constants obtained in the forward and reverse directions were used to calculate the activation energy of each step in the forward and reverse directions, respectively, according to eq 10. For eqs 9 and 10, k represents the rate being measured (k_H or k_{cat}), k_i is the rate constant of the reaction step, E_a is the experimental activation energy, T is the temperature in kelvin, R is the gas constant (1.98 cal mol^{-1}), A represents a pre-exponential factor that correlates collision frequency and the proper orientation of colliding molecules with the rate of the reaction,[21] and κ_B and h are Boltzmann's and Planck's constants, respectively. It is important to note that the activation energy and the enthalpy of activation are related by the equation $E_a = \Delta H^{\ddagger} + RT$.[22]

$$\Delta G^{\ddagger} = -RT[\ln(k_i) - \ln(\kappa_B T/h)] \quad (10)$$

To investigate the pH dependence of the chemical step, we performed single-turnover experiments from pH 5.5 to 7.5. For the reactions at different pH values, 100 mM MES with 50 mM KCl was utilized for pH values of 5.5−6.5 and 100 mM HEPES with 50 mM KCl was used for pH values of 6.5−7.5. Data for single turnovers at each pH were collected at saturating enzyme concentrations and analyzed as mentioned above, and the k_H values obtained were replotted as a function of pH and fitted to eq 11

$$\log y = \log[C/(1 + K_b/H)] \quad (11)$$

where y is the kinetic parameter, C is the pH-independent value of y, H is the proton concentration, and K_b is the apparent basic dissociation constant for ionizing groups.

Global Fitting of Data. Fluorescence stopped-flow data with more than one transient phase and data from experiments with concentration series were fit globally by regression analysis based upon numerical integration of the rate equations using KinTek Global Kinetic Explorer version 2.2 (KinTek Corp., Austin, TX). For different ligand concentrations, scaling factors were included in the data fitting process, and estimates for errors on parameters were derived by nonlinear regression and by FitSpace confidence contour analysis.[23,24]

Analysis of the Kinetic Scheme using Markov Chains. Continuous-time Markov chains (CTMCs) were generated, where rates or frequencies of occurrence over time are used. To generate CTMCs, a vector (i.e., an array of numbers) is multiplied by a matrix, where the rates of the kinetic scheme are defined for all existent enzyme forms. The matrix representing the kinetic scheme with all possible connections between enzyme forms was generated using KApattern.[25] Once the matrix was defined, a direct method (a linear system of equations) was used to calculate the stationary regime, e.g., the stage at which the system was simulated for a sufficiently large amount of time until changes no longer occurred. The result of this computation provided the probability of permanence for each state. The computation of such results was conducted by executing an online application available for free access. For this work, because nine enzyme forms were present, the matrix had 9 × 9 positions, which corresponds to the solution of a linear system of 11 unknown variables.[26] Concentrations of substrates and products were calculated assuming a K_{eq} of 5.06 × 10^7.[7,8]

RESULTS AND DISCUSSION

Multiple-Turnover Studies. Previously, it was demonstrated by the analysis of kinetic isotope effects under steady-state and single-turnover conditions that the isotope effect on the chemical step ($^D k_H$) and $^D(V/K_{DHF})$ were of equal magnitude, both being larger than $^D V$. This suggests that a step after chemistry is contributing to the rate of the reaction, decreasing the magnitude of $^D V$. Thus, it is likely that a step involved in product release is determining the rate of the reaction, which would be observed as a burst of product formation in a multiple-turnover experiment.[7,21,27,28] Figure 1A shows that, indeed, a small burst was observed when absorbance changes during turnover were monitored. The linear phase had a rate of 2.3 ± 0.1 s^{-1}, in good agreement with the k_{cat} obtained under steady-state conditions (2.5 ± 0.2 s^{-1}). The first exponential phase had a small amplitude, and simulations conducted with KinTek Global Kinetic Explorer demonstrated that if the rates of chemistry and product release are comparable in magnitude, the distinction between the exponential phase and the linear phase becomes troublesome, and the fitting might result in an incorrect determination of both rates. Moreover, it was clear

dx.doi.org/10.1021/bi200608n | Biochemistry 2011, 50, 7045−7056

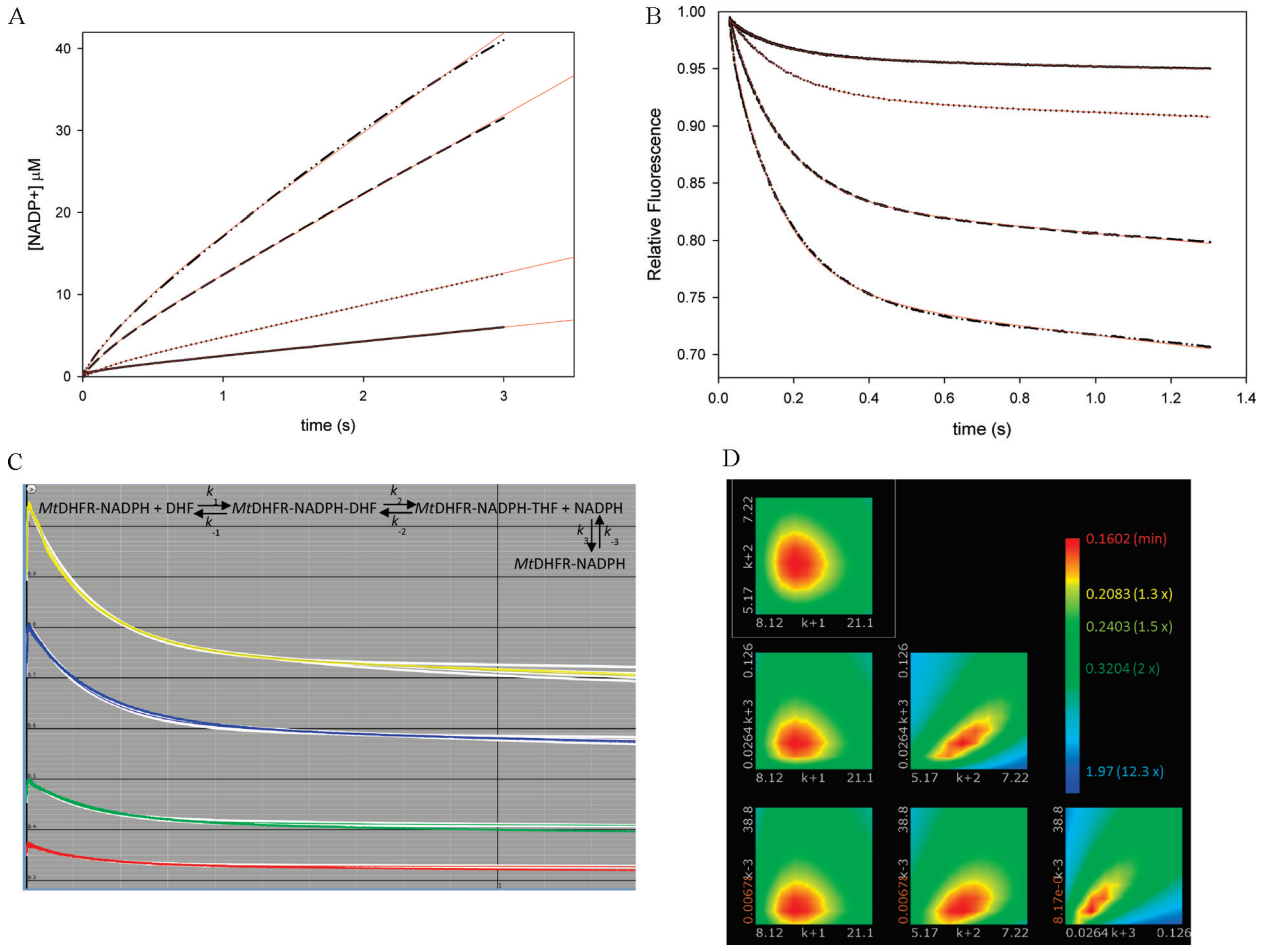

Figure 1. Pre-steady-state burst of product formation. The reaction was conducted with 100 μM DHF, 100 μM NADPH, and 1 (—), 2 (···), 5 (---), and 7 μM *Mt*DHFR (—·—). (A) The decrease in absorbance at 340 nm due to NADPH consumption was monitored, and the change in absorbance was converted into product formation by using an extinction coefficient of 11800 M^{-1} cm^{-1}.[18] The line is a fit to eq 4, yielding a steady-state rate constant of 2.3 ± 0.1 s^{-1}. (B) Fluorescence decrease due to NADPH consumption. The signal was obtained by excitation at 280 nm, and emission at 450 nm by fluorescence energy transfer caused by enzyme-bound NADPH. The larger amplitude of the burst phase allowed a better estimation of the burst rate; the line is a fit to eq 4, resulting in a burst rate constant of 7.4 ± 0.3 s^{-1}. (C) Global fit of the burst data shown in panel B with different concentrations of *Mt*DHFR (from bottom to top, 1, 2, 5, 7 μM) to the mechanism shown in the figure. The white contour represents fits of data within the parameter boundaries, so that all of the reasonable fits to the data are superimposed with the data and the best fit. (D) FitSpace confidence contours[24] for the global fit of the burst data. To avoid excessive fluctuation of kinetic parameters, the value for k_{-2} was fixed at 0.0004 s^{-1}, and the values for k_1 and k_{-1} were linked on the basis of a K_d of 2 μM for DHF.

that the amplitude of the burst was smaller than the concentration of active sites, suggesting that the rates of chemistry and product release are comparable or that an internal equilibrium is decreasing the burst amplitude.[29] To increase the magnitude of the signal obtained and more accurately estimate the rate of the exponential phase, multiple-turnover experiments monitoring FRET due to NADPH bound to the *Mt*DHFR were measured (Figure 1B). These data showed a much more distinctive burst of product formation, and the rate for the exponential phase was 7.4 ± 0.3 s^{-1}, which can be a good estimate of the rate of chemistry (k_H) even though it is slightly larger than the k_H value obtained in single-turnover experiments (see below). This value is in agreement with the fact that the observed burst rate is greater than or equal to the rate of the chemical reaction, being a function of forward and reverse rates of chemistry plus the rate of product release.[29] Figure 1C demonstrates the global fitting of the FRET burst data to the most simple plausible mechanism shown in the figure using KinTek Global Kinetic Explorer, and Figure 1D shows the FitSpace error contour analysis demonstrating that the rate of the burst phase is most likely between 5.17 and 7.22 s^{-1}.[24] Unfortunately, the amplitude of the burst kinetics using FRET cannot be used to calculate active site concentrations, since there is a complex and often nonlinear relationship between the FRET signal obtained and the amount of enzyme–ligand complex being formed.[30]

Single-Turnover Experiments. To obtain information about the rate of the hydride transfer step at different pH values and temperatures, as well as to determine the rate constants for binding of DHF to the *Mt*DHFR-NADPH binary complex, experiments under single-turnover conditions were performed. In these experiments, a biphasic transient was observed, consisting of a first fast concentration-dependent phase with a negative amplitude attributed to DHF binding, followed by a slower fluorescence decay caused by NADPH consumption. The enzyme concentration dependency of the observed rate constant of this second phase showed saturation behavior permitting the maximal chemistry rate constant to be estimated (5.8 ± 0.3 s^{-1}). This value is very similar to the

dx.doi.org/10.1021/bi200608n | *Biochemistry* 2011, 50, 7045–7056

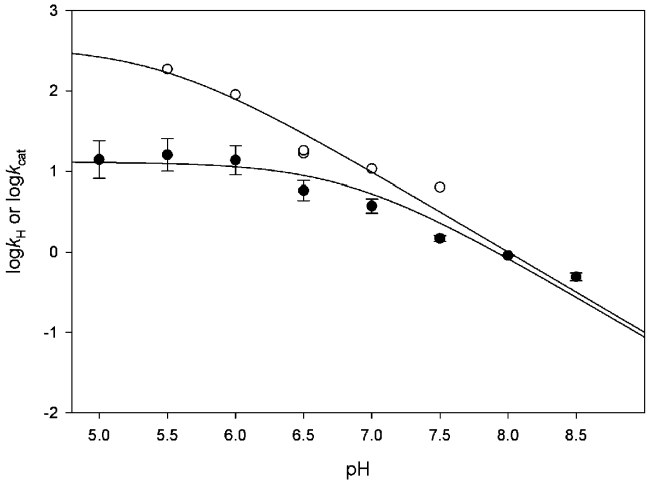

Figure 2. pH dependence of k_{cat} (●) and k_H (○). For pH values of 5.0−6.5, 100 mM MES with 50 mM KCl was utilized, and for pH 6.5−8.5, 100 mM HEPES with 50 mM KCl was used. The lines represent fits to eq 11, to give a k_H profile pK_a of 5.4 ± 0.3 and a k_{cat} profile pK_a of 6.8 ± 0.2. Values for k_{cat} and k_H are in inverse seconds.

chemistry rate measured in the burst experiments. To further investigate the hydride transfer step, single-turnover experiments were conducted at different pH values. Figure 2 compares the pH dependence of k_H and k_{cat}, and fitting to eq 11 yielded pK_a values of 6.8 ± 0.2 for k_{cat} and 5.4 ± 0.3 for k_H. As expected for a reaction in which a step after the chemical step is at least partly rate-limiting, there is an outward shift of the pK_a observed on the k_{cat} profile.[31] In addition, it is clear that chemistry becomes increasingly rate-limiting as the pH becomes higher than 6.0, corroborating previous studies that showed a kinetic isotope effect close to unity at acidic pH but increasing in magnitude at more basic pH values.[7] A similar pattern was observed in the *Ec*DHFR, but higher pK_a values were observed for this enzyme (pK_a = 6.5 for k_H, and pK_a = 8.5 for k_{cat}).[8] The contribution of the chemical step to the turnover rate was additionally assessed by measuring the dependence of k_H and k_{cat} on temperature. Activation energies of 11.7 ± 0.2 and 13.2 ± 0.3 kcal/mol were obtained for k_{cat} and k_H, respectively (Figure S18 of the Supporting Information). The calculation of the magnitude of the Gibbs free energetic barrier based on the rate constants measured for the forward and reverse rates of chemistry yielded a value of 15.1 kcal/mol, very similar to the activation energy measured by temperature studies.[23] The fact that the activation energies for k_H and k_{cat} are very comparable implies that the energetic barrier imposed by the chemical step is a significant contributor to the overall turnover rate. For comparison, the activation energies for the *Ec*DHFR-catalyzed reaction are 6.7 and 11.4 kcal/mol for k_H and k_{cat}, respectively, under similar experimental conditions.[32] These values are consistent with the much faster hydride transfer step in the *E. coli* enzyme and with the fact that chemistry has a small contribution for the turnover rate at neutral pH values. Additional information about the temperature studies is available in the Supporting Information.

Binding Kinetics. The observation of a burst of product formation argues that another step or other steps occurring after the hydride transfer contribute to the turnover rate. Therefore, binding and dissociation experiments were conducted to identify these steps. The association and dissociation rate constants for DHF and THF were measured by monitoring protein fluorescence and FRET (Table 1). Both binding of THF to *Mt*DHFR-NADPH and binding of THF to *Mt*DHFR-NADP$^+$ resulted in biphasic binding transients (Figure 3A), with the k_{obs} of the fast phase being linearly dependent on the concentration of THF followed by a slower phase with a k_{obs} showing hyperbolic concentration dependence (Figure 3B). Hence, THF binds to both complexes via a two-step binding mechanism with a fast bimolecular association step followed by a slow isomerization step. Fitting of the replots of the observed rate constants allowed the determination of the four rate constants of a two-step binding mechanism for each complex (Table 2 and Figures S7 and S9 of the Supporting Information; see Experimental Procedures for the equations used for data fitting). The likelihood of the two-step binding mechanism was tested by global fitting of the data.[23] Table 2 compares the rates obtained by analytical fitting and global fitting and summarizes the experiments conducted to determine each of the rate constants.

These data suggest that release of THF from both ternary complexes (*Mt*DHFR-NADPH-THF and *Mt*DHFR-NADP$^+$-THF) is a biphasic process with a slow isomerization step followed by a fast dissociation step. The slowest step in the release of THF from both complexes is a slow isomerization between a tightly bound and a loosely bound complex,

Table 1. Binding and Dissociation Rate Constants

Binding Rate Constants					
enzyme species	ligand	k_1 (μM^{-1} s^{-1})	k_{-1} (s^{-1})	k_2 (s^{-1})	k_{-2} (s^{-1})
*Mt*DHFR-NADPH	THF	7.3 ± 0.4	147 ± 2.5	4.3 ± 0.1	1.0 ± 0.1
*Mt*DHFR-NADP$^+$	THF	13.9 ± 3.2	127.1 ± 23.5	3.4 ± 0.3	2.3 ± 0.6
*Mt*DHFR-NADP$^+$	DHF	0.21 ± 0.02	2.7 ± 0.1	–	–
*Mt*DHFR-NADPH	DHF	22 ± 4	140 ± 30	–	–

Dissociation Rate Constants using the Competition Method			
enzyme species	ligand	competitor	k_{off} (s^{-1})
*Mt*DHFR-NADPH	THF	MTX	4.7 ± 0.1
*Mt*DHFR-NADPH	–	NADP$^+$	0.13 ± 0.01
*Mt*DHFR-NADP$^+$	–	NADPH	97.6 ± 4.1
*Mt*DHFR-NADP$^+$	DHF	NADPH	7.8 ± 0.1
*Mt*DHFR-NADPH	THF	NADP$^+$	1.7 ± 0.6
*Mt*DHFR-NADP$^+$	DHF	MTX	0.47 ± 0.04
*Mt*DHFR-NADP$^+$	THF	MTX	3.6 ± 0.3
*Mt*DHFR-NADP$^+$	THF	NADPH	8.0 ± 0.1

dx.doi.org/10.1021/bi200608n | *Biochemistry* 2011, 50, 7045−7056

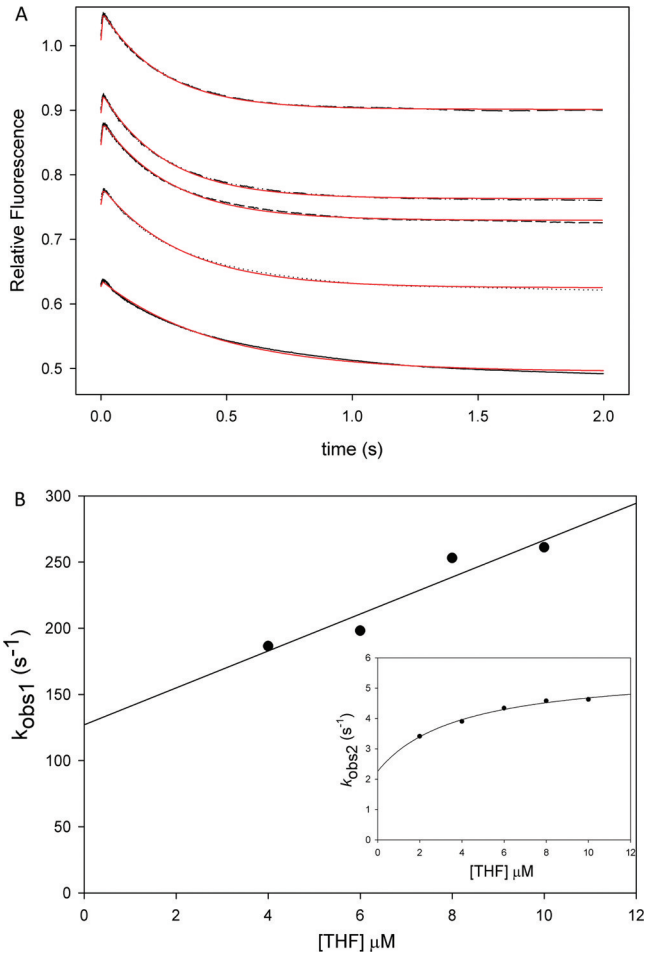

Figure 3. Binding of THF to *Mt*DHFR-NADP$^+$. (A) Increasing concentrations of THF [2 (—), 4 (···), 6 (---), 8 (—···—), and 10 (——) μM] were mixed with 0.5 *Mt*DHFR-NADP$^+$, monitoring the change in protein fluorescence (excitation at 280 nm and emission above 320 nm). Traces were fitted to a double-exponential equation (line, eq 3). (B) The observed rate constants obtained (s^{-1}) were plotted as a function of THF concentration, and the rate constants were obtained after fitting to eq 5 or 6 (inset). The lowest concentrations were excluded from replots to maintain pseudo-first-order conditions but were kept for the global fitting of the data (summarized in Table 2).

occurring at rates of 1.3 and 1.9 s^{-1} from *Mt*DHFR-NADPH-THF and *Mt*DHFR-NADP$^+$-THF, respectively. Both values are close to the steady-state turnover rate. The release of THF from *Mt*DHFR-NADPH-THF is the rate-limiting step in the kinetic sequences from *E. coli* DHFR (*Ec*DHFR), *Lactobacillus casei* DHFR (*Lc*DHFR), mouse DHFR (*m*DHFR), and *Pneumocystis carinii* (*Pc*DHFR).[8,10−12] In contrast to the results obtained here, the release of THF from ternary complexes occurs as a single bimolecular step for all previously characterized DHFRs.

In the catalytic cycle of the human DHFR (*Hs*DHFR), THF can be released first from the enzyme-product ternary complex, followed by DHF binding, NADP$^+$ release, and subsequent binding of NADPH to reinitiate the cycle. To rule out this possibility in the *Mt*DHFR kinetic sequence, binding of DHF to both *Mt*DHFR enzyme forms was investigated. The results obtained showed that the association of DHF with *Mt*DHFR-NADPH, to generate the catalytic productive complex, is fast and does not limit the turnover rate (Tables 1 and 2 and Figure S1 of the Supporting Information). Binding of DHF to the *Mt*DHFR-NADP$^+$ complex, on the other hand, is a single-step process with a slow association rate constant of 0.7 s^{-1} and thus is unlikely to occur during the catalytic cycle (Figure S15 of the Supporting Information). Rate constants for the formation of the dead-end *Mt*DHFR-NADP$^+$-DHF complex are shown in Scheme 2 and Tables 1 and 2.

Because *Mt*DHFR is purified in a complex with NADPH, and this tightly bound NADPH could not be removed without a loss of protein stability but only replaced by NADP$^+$, binding experiments that required free enzyme could not be performed. Given the extremely high affinity of *Mt*DHFR for phosphorylated pyridine nucleotides, it is unlikely that free enzyme exists for a long period of time in vivo.

Dissociation Kinetics Determined via Competition Experiments. Dissociation rate constants were measured by conducting competition experiments, where there is an equilibrium for the binding of two competing ligands, as shown in Scheme 3. The dissociation rate constant for ligand 1 can be measured as long as $k_2[L_2] \gg k_{-1}$, $k_1[L_1]$, and this condition is satisfied by using increasing concentrations of the competitor, ligand 2, until no change in the observed rate constant is seen.[33,34] Figure 4 shows the dependence of the rate constant for dissociation of NADPH from the *Mt*DHFR-NADPH complex on the concentration of NADP$^+$. Two processes that would generate free enzyme were evaluated, one being the fast NADP$^+$ dissociation [~98 s^{-1} (Figure S12 of the Supporting Information)] and the other being the very slow NADPH dissociation [0.13 s^{-1} (Figure S13 of the Supporting Information)]. Interestingly, all other dissociation rate constants thought to be relevant for the main catalytic pathway were of the same magnitude, ranging from 1.3 to 8.0 s^{-1} (Figures S4, S5, S8, S11−S13, S16, and S17 of the Supporting Information). Rate constants determined by dissociation, and binding experiments, are summarized in Table 1.

Reverse Reaction. The conversion of THF and NADP$^+$ to DHF and NADPH catalyzed by *Mt*DHFR was monitored by the increase in absorbance at 340 nm and analyzed by steady-state kinetics and single- and multiple-turnover experiments. The results show that both $k_{cat-rev}$ and $k_{chem-rev}$ have the same rate of 0.0004 s^{-1}, and consequently, no burst of product formation was observed (Figure S3 of the Supporting Information). This result indicates that the chemical step is virtually irreversible with an internal equilibrium constant for THF formation of approximately 1500, a value essentially equal to the one observed for the *Ec*DHFR-catalyzed reaction.[8] This result provides an explanation for the fact that kinetic isotope effects measured on k_{cat} exhibit a lower value than the ones measured for $^D(V/K_{DHF})$.[7] Because $^D(V/K_{DHF})$ reports on steps up to and including the first irreversible step, now known to be the chemical step, any decrease in observed kinetic isotope effects caused by product release does not affect the $^D(V/K_{DHF})$ but decreases the magnitude of ^DV isotope effects.

Catalytic Cycle of *Mt*DHFR and Comparison to Those of Other DHFRs. Measurement of association and dissociation rate constants of substrates and products to most possible enzyme forms as well as rates for the forward and reverse chemical steps allows the assignment of the pathway or pathways that the enzyme most likely follows during steady-state turnover. In this discussion, an important corollary of pre-steady-state kinetics must be reinforced: a rate constant of an elementary step in the main path of the reaction cannot be smaller than the overall reaction rate constant (k_{cat}). Thus, it is

Table 2. Comparison between Rate Constants Obtained by Analytical Fitting and Global Fitting[a]

rate constant	best-fit value, global fitting	lower boundary	upper boundary	value obtained by analytical fitting	experiment conducted
k_1	31.9 ± 0.5	25.6	45.4	22 ± 4	single turnover
k_{-1}	64.3 ± 0.1[b]	–	–	140 ± 30	single turnover
k_2	4.5 ± 0.1	3.18	6.17	5.8 ± 0.3	single turnover
k_{-2}	0.00056 ± 0.00003	0.00052	0.00068	0.0004 ± 0.00001	single turnover
k_3	7.3 ± 0.1	6.3	8.3	8.02 ± 0.02	NADPH competition
k_{-3}	109 ± 6	28	213	ND[d]	–
k_4	101	–	–	ND[d]	–
k_{-4}	1.1 ± 0.1	0.29	4.2	1.7 ± 0.6	$NADP^+$ competition
k_5	1.1 ± 0.1	0.9	1.2	4.7 ± 0.1	MTX competition
k_{-5}	1.5 ± 0.1	1.2	1.8	4.1 ± 0.2	THF binding
k_6	165.5 ± 4.6	106	632	147 ± 2	THF binding
k_{-6}	59 ± 2	38	223	7.4 ± 0.4	THF binding
k_7	1.7 ± 0.1	0.7	3.39	3.6 ± 0.3	MTX competition
k_{-7}	2.3 ± 0.1	2.1	2.5	3.4 ± 0.3	THF binding
k_8	78 ± 2	–	46.8	100 ± 23	THF binding
k_{-8}	38 ± 1	12.8	39.5	7.2 ± 0.4	THF binding
k_9	81 ± 2	64.8	101	98 ± 4	NADPH competition
k_{-9}[c]	268 ± 7	215	420	ND[d]	–
k_{10}	129 ± 4	66.1	252	ND[d]	–
k_{-10}	0.08 ± 0.01	0.07	0.09	0.13 ± 0.01	$NADP^+$ competition
k_{11}	0.7 ± 0.1	0.5	0.9	0.21 ± 0.01	DHF binding
				0.47 ± 0.04	MTX competition
k_{-11}	1.1 ± 0.1	0.2	2.1	2.7 ± 0.1	DHF binding
k_{12}	2.1 ± 0.2	0.5	9.1	7.8 ± 0.1	NADPH competition
k_{-12}	–	–	–	ND[d]	–
k_{13}	6.7 ± 0.3	4.98	12.1	ND[d]	–
k_{-13}	0.32 ± 0.04	0.0005	0.78	ND[d]	–

[a]The bimolecular steps have rate constants expressed in μM^{-1} s^{-1}, whereas unimolecular steps have rate constants in s^{-1}. [b]Linked to k_1 during global fitting, based on a K_{DHF} of 2 μM.[7] The value was not well constrained by the data if allowed to vary freely. [c]Linked to k_9 for global fitting, based on a K_{NADP} of 0.33 μM.[7] [d]Not determined experimentally.

Scheme 2. Formation of the Dead-End *Mt*DHFR-$NADP^+$-DHF Complex[a]

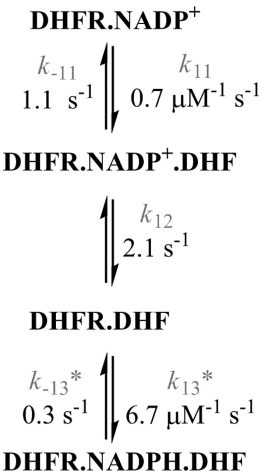

[a]The values of the rate constants were obtained by global fitting of the data with KinTek Global Kinetic Explorer. Rate constants not experimentally measured are denoted with asterisks.

Scheme 3. Events Occurring during a Competition Experiment with Ligand L_2 Used as a Competitor To Determine the Rate Constant for Dissociation of L_1 from the E-L_1 Complex

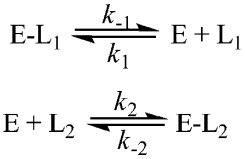

assumed that a step with a rate constant smaller than k_{cat} is not part of the main path followed by the overall reaction.[20] Considering this restriction, a mechanism that includes dissociation of NADPH from any enzyme form must be discarded, because NADPH dissociation is a slow process from all complexes analyzed (ranging from 0.078 to 1.1 s^{-1}), so that the catalytic cycle of the *Mt*DHFR starts with *Mt*DHFR-NADPH as a complex. Comparison with other DHFRs shows that some of them have a relatively high k_{off} for dissociation of NADPH from DHFR-THF-NADPH, so it is possible that dissociation of NADPH from this complex occurs during turnover (k_{off} values of 85 s^{-1} for *E. coli*,[8] 480 s^{-1} for *Streptococcus pneumoniae*,[14] and 100 s^{-1} for humans[9]). Next, DHF binds to *Mt*DHFR-NADPH to form the productive ternary complex, whose formation is fast and unlikely to be rate-limiting, unless the concentration of DHF is in the submicromolar range. After the *Mt*DHFR-NADPH-DHF ternary complex is formed, the chemical step occurs at a relatively slow rate of ~5 s^{-1} compared to the rates of other DHFRs at pH 7.5 [e.g., k_H equal to 250 s^{-1} (*Ec*DHFR[8]), 500 s^{-1} (*m*DHFR[10]), and 1360 s^{-1} (*Hs*DHFR)[9]]. To further illustrate the diversity of kinetic schemes for DHFRs from different species, in *Sp*DHFR, the chemical step is preceded by a rate-determining conformational change, and the bifunctional thymidilate synthase-DHFR from

dx.doi.org/10.1021/bi200608n | *Biochemistry* 2011, 50, 7045–7056

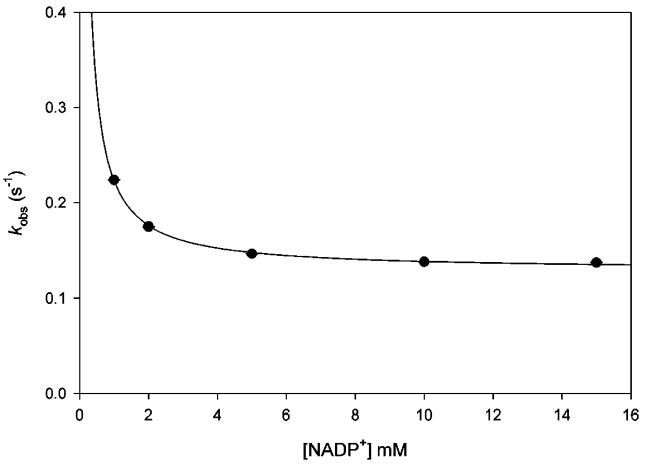

Figure 4. $NADP^+$ competition with *Mt*DHFR-NADPH. Increased concentrations of $NADP^+$ were mixed with the *Mt*DHFR-NADPH complex. According to Scheme 3, at infinite concentrations of the competitor ($NADP^+$), the rate obtained is the dissociation rate constant (k_{off}) for ligand 1 (NADPH). The line is a hyperbolic fit, yielding a k_{off} of 0.13 ± 0.01 s^{-1}.

Leishmania major undergoes a rate-determining conformational change when free of ligands or bound to THF.[13,14] As previously shown,[7] kinetic isotope effects greater than 1 and of practically equal magnitudes were obtained for $^D(V/K_{DHF})$ and ^Dk_H, strongly suggesting that a conformational change prior to the chemical step is not limiting k_H in *Mt*DHFR. Following the chemical step, which is also the first "kinetically" irreversible step in the sequence, the enzyme-products complex (*Mt*DHFR-$NADP^+$-THF) can decompose via two pathways of product release. In the first pathway, $NADP^+$ is released and NADPH binds, followed by a biphasic release of THF in which a rate-limiting isomerization step is followed by fast THF dissociation, generating the initial *Mt*DHFR-NADPH complex (pathway A, Scheme 4). Pathways with the same order of product release, which is known as a "nucleotide exchange pathway", have been found for the majority of DHFRs.[8,10−12] Alternatively, the *Mt*DHFR-$NADP^+$-THF complex can proceed to first release THF in a biphasic process, where a rate-limiting isomerization is followed by fast $NADP^+$ dissociation to form the apoenzyme, which then rapidly binds NADPH to yield the initial *Mt*DHFR-NADPH complex (pathway B, Scheme 4). This pathway is rather unique, and a similar sequence was suggested to be a secondary route followed by the *Hs*DHFR at saturating NADPH concentrations and a very low concentration of DHF.[9]

The kinetic sequence shown here (Scheme 4) includes isomerization steps preceding the release of THF from *Mt*DHFR-NADPH and *Mt*DHFR-$NADP^+$ complexes, and the likelihood of these mechanisms was evaluated by global fitting of the results of all binding and dissociation experiments, which showed that the model is well-constrained by the data (Table 2). This is the first report of a biphasic rate-limiting product release for a DHFR. It was previously demonstrated for *Ec*DHFR that an NMR-determined exchange rate constant for residues surrounding the folate binding pocket correlates precisely with the rate constant for the release of THF from *Mt*DHFR-NADPH, the rate-limiting step for this reaction.[6] Although this rate-determining step in the *Ec*DHFR kinetic sequence seems to be coupled to a conformational change, binding experiments demonstrated that THF binds in a single-step manner to the *Ec*DHFR, so that the observed first-order rate constant increased linearly with increasing THF concentration, showing no sign of saturation. While it is tempting to suggest the same conformational change is limiting THF release in the *Mt*DHFR reaction, no information about the conformational dynamics of this protein is available.

Likelihood of Parallel Pathways for Product Release. The comparable magnitudes of rate constants obtained for both pathways of product release, together with the fact that none of the slowest steps in both pathways is equal to k_{cat} (k_{cat} = 2.3 s^{-1}, THF release equal to 1.1 s^{-1} from *Mt*DHFR-NADPH-THF in pathway

Scheme 4. Kinetic Scheme for the *Mt*DHFR-Catalyzed Reaction[a]

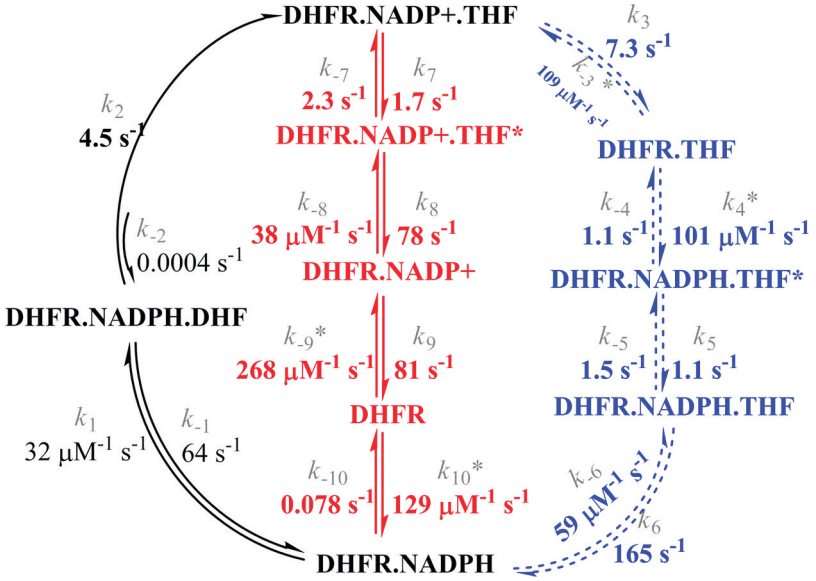

[a]Pathway A is represented in the outward circular portion in dashed lines, while pathway B is shown in the center. The values of the rate constants were obtained by global fitting of the data with KinTek Global Kinetic Explorer. Rate constants not experimentally measured are denoted with asterisks.

dx.doi.org/10.1021/bi200608n | *Biochemistry* 2011, 50, 7045−7056

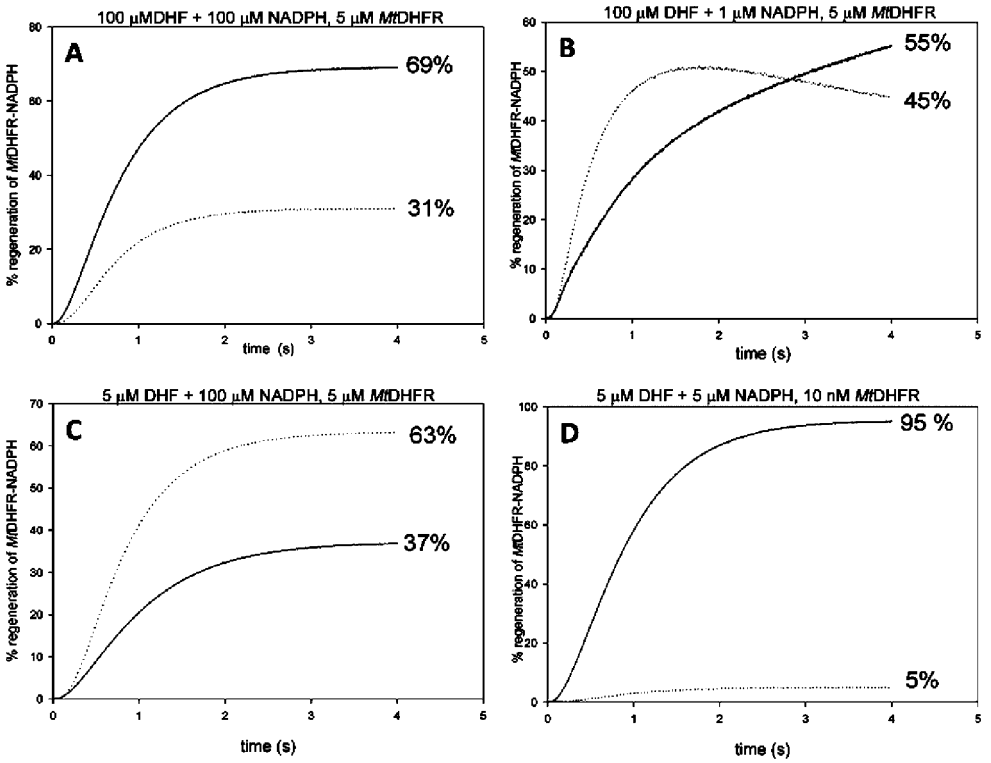

Figure 5. Product release through two parallel pathways. Simulations conducted using KinTek Global Kinetic Explorer with (A) saturating concentrations of both substrates (100 μM) and 5 μM *Mt*DHFR, (B) 100 μM DHF, 1 μM NADPH, and 5 μM *Mt*DHFR, (C) 5 μM DHF, 100 μM NADPH, and 5 μM *Mt*DHFR, and (D) simulating typical steady-state conditions with 5 μM DHF, 5 μM NADPH, and 10 nM *Mt*DHFR. The dotted line represents the fact that *Mt*DHFR-NADPH is being generated by pathway A, and the solid line indicates that pathway B generated *Mt*DHFR-NADPH.

A and 3.3 s^{-1} from *Mt*DHFR-$NADP^+$-THF* in pathway B), suggest a contribution from both pathways to k_{cat}.

To better explore this hypothesis, we conducted simulations using KinTek Global Kinetic Explorer. The two potential pathways for product release were evaluated assuming that if the enzyme-products complex followed pathway A (with $NADP^+$ released first) an enzyme form called E-NADPHa would be formed, and when the enzyme-products complex followed pathway B, an enzyme form called E-NADPHb would form. By conducting this simulation, one can imagine that after several turnovers the reaction would reach completion, and the final concentrations of E-NADPHa and E-NADPHb would be a way of quantifying how many turnovers occurred via pathway A or B. The simulation was conducted at varying initial concentrations of substrates to estimate how different conditions can influence the pathway followed. Figure 5A shows that, when both substrates are saturating, 31% of the E-NADPH complex was generated by following pathway A and 69% of the generated E-NADPH was due to turnover following pathway B. Figure 5C shows that the only condition under which pathway A was preferred was when the concentration of DHF was subsaturating, and equimolar with respect to the concentration of the enzyme.

An evaluation of both pathways in terms of free energy was conducted by generating the reaction coordinate of the NADPH-dependent reduction of DHF by *Mt*DHFR at pH 7.5 and 25 °C. The Gibbs free energy barrier for each reaction step was calculated using eq 10. Substrate concentrations were taken to be 1 M, and concentrations of products were calculated on the basis of the K_{eq} of 5.06×10^7 between substrate and product.[7] The *Mt*DHFR-NADPH state was taken as the reference state. Figure 6 shows that pathway A has the two most stable intermediates in the sequence, which are followed by THF dissociation (*Mt*DHFR-NADPH-THF and *Mt*DHFR-NADPH-THF*), whereas

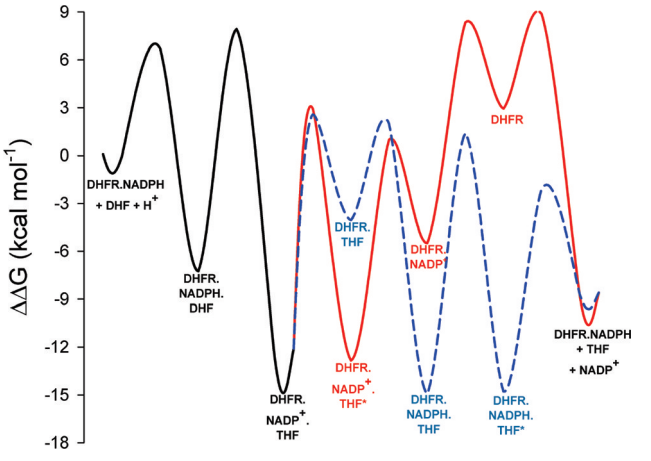

Figure 6. Energy profile comparing the two pathways for product release. The energy barrier for each step was calculated using eq 10.[38] Substrate and product concentrations were 1 and 1.26 M, respectively, calculated on the basis of the equilibrium constant for the reaction.[7] The profile shown with a dashed line represents pathway A, and the profile showed with a solid line represents pathway B.

dx.doi.org/10.1021/bi200608n | *Biochemistry* 2011, 50, 7045–7056

pathway B includes the formation of the high-energy apoenzyme (DHFR) and one relatively stable intermediate (*Mt*DHFR-NADP$^+$-THF*).

To quantify the relative stability of each intermediate in the kinetic sequence and to substantiate the intuitive notion that on the basis of the magnitudes of the rate constants a majority of enzyme-products complex will likely accumulate and then partition almost equally toward *Mt*DHFR-NADP$^+$-THF* and *Mt*DHFR-THF, a mathematical analysis was conducted by combining KApattern[25] and Markov chains. A Markov chains (MCs) approach is a well-known mathematical formalism used in many fields with a very broad application, in which states and transitions among states according to rates that were observed in the system under study are utilized. In this work, the system consists of enzymes species (states) and rate constants (rates). The purpose of MCs is to calculate the permanence probabilities when the system remains stable assuming that it was simulated for a long period of time, a situation analogous to that in which the reaction has reached equilibrium. MCs have the Markov property, which asserts that the only information needed to find the next state is present in the current state and is the most fundamental property in MCs, stating that the states visited in the past do not influence how the future state will be chosen.[26] For the

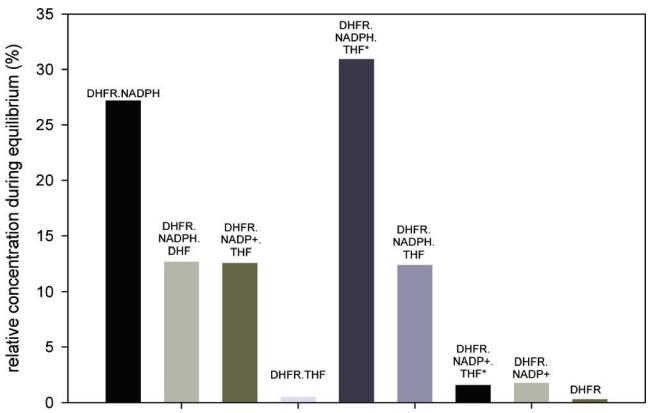

Figure 7. Accumulation of enzyme intermediates in equilibrium, analyzed by the generation of continuous time Markov chains (CTMCs). A matrix representing the kinetic scheme with all possible connections between enzyme forms was generated using KApattern,[25] and the system was simulated until equilibrium was reached. The result is the probability of permanence in each enzyme form, when the reaction has reached equilibrium. Concentrations of substrates and products were calculated assuming a K_{eq} of 5.06×10^7.[7,8]

kinetic scheme investigated here, Figure 7 illustrates that the enzyme-products complex accumulates to a certain extent, given that the reverse chemical rate ($k_{chem-rev}$; see discussion above) is negligible, and the rates driving the dissolution of this complex are similar in magnitude (1.7 and 7.3 s^{-1}) to the forward chemistry rate constant (5 s^{-1}). After the *Mt*DHFR-THF complex is formed, the rapid binding of NADPH causes the formation of the *Mt*DHFR-NADPH-THF* complex, whose isomerization prior to THF release represents the rate-limiting step in this pathway (pathway A). The isomerization of the enzyme-products complex prior to THF dissociation, on the other hand, is the rate-limiting step of pathway B. After this isomerization occurs, all subsequent steps are in rapid equilibrium, except for binding of NADPH to the enzyme, which drives the reaction forward to restart a new cycle. The fact that none of the enzyme intermediates from pathway B are present in large amounts during equilibrium illustrates the fact that once the *Mt*DHFR-NADP$^+$-THF complex isomerizes, it is driven to regenerate the initial *Mt*DHFR-NADPH complex. This is in contrast with the situation in pathway A, where the formation of two very stable intermediates traps the enzyme in nonproductive forms. These results, taken together with the energy profile (Figure 6), show that the two very stable intermediates in pathway A, together with the *Mt*DHFR-NADPH complex, the enzyme-substrates complex, and the initial enzyme-products, complex are the most abundant enzyme forms in equilibrium.

It has been hypothesized in the literature that intracellular levels of NADPH and NADP$^+$ are responsible for the natural selection of enzymes that bind with different affinities to the reduced and oxidized forms of the pyridine cofactor. In the cytoplasm of eukaryotes, NADP$^+$ is present at no more than 1% of the concentration of NADPH,[9] whereas the concentration of these nucleotides is comparable in prokaryotes, like *E. coli*,[35] and can explain why *Ec*DHFR binds NADPH more tightly than NADP$^+$ (dissociation constants are 0.17 and 23 μM for NADPH and NADP$^+$, respectively). Moreover, once the *Ec*DHFR-NADP$^+$ complex is formed it can rapidly bind DHF and generate a very stable dead-end complex, which would not be selectively advantageous if k_{cat} was under selective pressure. The *Hs*DHFR binds to both nucleotides with similar affinity, but the intracellular difference in concentration between NADPH and NADP$^+$ makes unproductive pathways that require NADP$^+$ binding to the apoenzyme negligible. In the case of *Mt*DHFR assuming that the concentrations of NADPH and NADP$^+$ are comparable,[36] even though NADP$^+$ binding is in rapid equilibrium with the free enzyme, NADPH binding generates a very stable enzyme complex whose dissociation is extremely slow, so that binding of NADPH is favored over binding of NADP$^+$ to the apoenzyme. The only other DHFR that possesses a kinetic sequence that passes through free enzyme is a mutant of *Hs*DHFR in which the widely conserved phenylalanine 34 was replaced with an alanine.[37] This mutant enzyme has an ordered product release, with THF being released first, followed by NADP$^+$. It is important to point out that the *Mt*DHFR has this phenylalanine.

Steady-State Turnover. A vital check of the validity of a model is whether it can account for the events that occur during steady-state turnover. To better corroborate the kinetic scheme in which two parallel pathways exist for *Mt*DHFR and the fact that k_{cat} represents a combination of the rates of both pathways, KApattern was utilized to generate rate equations for each of the pathways, thus yielding k_{cat} values for each parallel pathway. In the process of obtaining the rate equations, the concentrations of products were assumed to be zero. The rate equations were rearranged to the form of eq 12, describing a sequential kinetic mechanism, so that k_{cat} could be isolated. In this equation, v is the velocity, E_t is the total concentration of enzyme, k_{cat} is the turnover rate, A and B are the substrate concentrations, K_{ia} is the inhibition constant for substrate A, K_a is the Michaelis

constant for substrate A, and K_b is the Michaelis constant for substrate B.

$$v/E_t = k_{cat}AB/(K_{ia}K_b + K_bA + K_aB + AB) \quad (12)$$

For pathway A

$$v/E_t = k_6[\text{DHFR-NADPH-THF}] / \left[\sum (\text{all enzyme forms in path A})\right]$$

so that

$$k_{cat} = k_6k_5k_3k_2 / [k_6k_5(k_{-2} + k_3 + k_2) + k_3k_2(k_6 + k_5 + k_{-5})]$$

Similarly, for pathway B

$$v/E_t = k_5[\text{DHFR-NADP}^+] / \left[\sum (\text{all enzyme forms in path B})\right]$$

so that

$$k_{cat} = k_6k_5k_3k_4k_2k_1 / [k_1k_6k_2k_5(k_{-3} + k_4) + k_5(k_{-2}k_{-3} + k_{-2}k_4 + k_4k_3) + k_3k_2k_5k_4k_2]$$

Finally, the rate constants obtained in the global fitting (Table 2) were utilized to obtain k_{cat} values of 0.90 s^{-1} for pathway A and 2.0 s^{-1} for pathway B. These values are in good agreement with the values obtained under steady-state conditions, considering that for this calculation a situation analogous to the one depicted in Figure 5D is occurring, where turnover through path B predominates. Furthermore, the kinetic sequence presented here corroborates the previously proposed kinetic mechanism for this enzyme, i.e., steady-state random, because the rate of chemistry is comparable to the rates of substrate dissociation and product release is random.

A final test of the events that occur during steady-state turnover was conducted by calculating the equilibrium difference in Gibbs free energy (ΔG) for this reaction based on the proposed reaction coordinate starting from the *Mt*DHFR-NADPH state using the rate constants obtained experimentally and comparing this to the ΔG calculated from the K_{eq} for this reaction.[7] The values are −9.5 kcal/mol (ΔG obtained from K_{eq}) and −8.7 and −8.5 kcal/mol for ΔG values calculated using the rate constants from pathways A and B, respectively. These values differ by only 1 kcal/mol, additionally assuring the robustness of the sequence proposed here.

Table 3. Equilibrium Dissociation Constants (all in micromolar)[a]

enzyme species	ligand	K_{ov}[b]	K_d measured	K_{ov} (global fit values)
*Mt*DHFR-NADPH	THF	4.1 ± 0.9	1.4 ± 0.4[c]	1.2 ± 0.1
*Mt*DHFR-NADP$^+$	THF	1.2 ± 1.5	1.1 ± 0.1[c]	1.2 ± 0.4
*Mt*DHFR-NADP$^+$	DHF	12.1 ± 1.3[e]	1.9 ± 1.3[d]	1.6 ± 0.1
*Mt*DHFR-NADPH	DHF	6.4 ± 1.8[e]	ND	5.1 ± 0.1

[a]For additional information, see Figures S6, S9, and S14 of the Supporting Information. [b]K_{ov} is the dissociation constant calculated using eq 7 or k_{off}/k_{on}. [c]Obtained from equilibrium binding experiments. [d]Obtained from the analysis of the amplitudes of binding transients in stopped-flow fluorescence measurements. See the Supporting Information for a description of the equation used. [e]Calculated from k_{off}/k_{on} using values obtained in the binding experiments.

Summary. In this work, the kinetic sequence of the *Mt*DHFR-catalyzed reaction was studied by a combination of equilibrium binding, pre-steady-state kinetics, global fitting, and simulation. This reaction was shown to follow two parallel pathways, one similar to those of other DHFRs where $NADP^+$ is released first, followed by NADPH binding and THF release, and an alternative pathway in which THF and $NADP^+$ are released to transiently form free enzyme, to which NADPH binds reinitiating the cycle. The kinetic sequence with parallel pathways describes the steady-state behavior of *Mt*DHFR, being further validated by the calculation of steady-state k_{cat} using the rate constants obtained in this work, and the Markov models that demonstrate that the accumulation of very stable enzyme intermediates prevents turnover via a single path. This is the first DHFR possessing two equally relevant kinetic pathways, with the unique feature that one of these pathways passes through the free enzyme (Table 3).

■ ASSOCIATED CONTENT

Ⓢ Supporting Information

A complete description of pre-steady-state experiments and analytical data fitting and an extended analysis of temperature studies. This material is available free of charge via the Internet at http://pubs.acs.org.

■ AUTHOR INFORMATION

Corresponding Author

*Department of Biochemistry, Albert Einstein College of Medicine, 1300 Morris Park Ave., Bronx, NY 10461. Phone: (718) 430-3095. Fax: (718) 430-8565. E-mail: cczekster@gmail.com or anvdmb@gmail.com.

Funding

This work was supported by the National Institutes of Health (AI33696) and the Einstein-Montefiore CFAR (National Institutes of Health Grant AI-515109), and A.V. was the recipient of a Belgian American Educational foundation fellowship.

■ ACKNOWLEDGMENTS

We thank Dr. Ricardo M. Czekster [Pontifícia Universidade Católica do Rio Grande do Sul (PUCRS)] for insightful discussions using Markov models and Dr. Kenneth A. Johnson (University of Texas at Austin, Austin, TX) for his help with data interpretation and analysis using KinTek Global Kinetic Explorer.

■ ABBREVIATIONS

TB, tuberculosis; *m*DHFR, DHFR from mouse; MDR-TB, multidrug resistant tuberculosis; XDR-TB, extensively drug resistant tuberculosis; *Mt*DHFR, dihydrofolate reductase from *M. tuberculosis* H37Rv; DHF, dihydrofolate; THF, tetrahydrofolate; NADPH, nicotinamide adenine dinucleotide phosphate (reduced form); $NADP^+$, nicotinamide adenine dinucleotide phosphate (oxidized form); MTX, methotrexate;

dTMP, deoxythymidine monophosphate; FRET, fluorescence resonance energy transfer; k_{obs}, observed rate constant; k_{cat}, steady-state turnover number; $k_{cat-rev}$, steady-state turnover number for the reverse reaction; k_H, rate constant of chemistry for the forward reaction; $k_{chem-rev}$, rate constant of chemistry for the reverse reaction; k_{on}, association rate constant; k_{off}, dissociation rate constant; KIE, kinetic isotope effect; $^{D}k_H$, kinetic isotope effect in the chemical step; *Ec*DHFR, DHFR from *E. coli*; *Sp*DHFR, DHFR from *S. pneumoniae*; MCs, Markov chains.

REFERENCES

(1) Kompis, I. M., Islam, K., and Then, R. L. (2005) DNA and RNA synthesis: Antifolates. *Chem. Rev. 105*, 593−620.

(2) McGuire, J. J. (2003) Anticancer antifolates: Current status and future directions. *Curr. Pharm. Des. 9*, 2593−2613.

(3) Hitchings, G. H. Jr. (1989) Nobel lecture in physiology or medicine—1988. Selective inhibitors of dihydrofolate reductase. *In Vitro Cell. Dev. Biol. 25*, 303−310.

(4) Ionescu, R. M., Smith, V. F., O'Neill, J. C. Jr., and Matthews, C. R. (2000) Multistate equilibrium unfolding of *Escherichia coli* dihydrofolate reductase: Thermodynamic and spectroscopic description of the native, intermediate, and unfolded ensembles. *Biochemistry 39*, 9540−9550.

(5) Hammes-Schiffer, S., and Benkovic, S. J. (2006) Relating protein motion to catalysis. *Annu. Rev. Biochem. 75*, 519−541.

(6) Boehr, D. D., McElheny, D., Dyson, H. J., and Wright, P. E. (2006) The dynamic energy landscape of dihydrofolate reductase catalysis. *Science 313*, 1638−1642.

(7) Czekster, C. M., Vandemeulebroucke, A., and Blanchard, J. S. (2011) Kinetic and Chemical Mechanism of the Dihydrofolate Reductase from *Mycobacterium tuberculosis*. *Biochemistry 50*, 367−375.

(8) Fierke, C. A., Johnson, K. A., and Benkovic, S. J. (1987) Construction and evaluation of the kinetic scheme associated with dihydrofolate reductase from *Escherichia coli*. *Biochemistry 26*, 4085−4092.

(9) Appleman, J.R., Beard, W. A., Delcamp, T. J., Prendergast, N. J., Freisheim, J. H., and Blakley, R. L. (1990) Unusual transient- and steady-state kinetic behavior is predicted by the kinetic scheme operational for recombinant human dihydrofolate reductase. *J. Biol. Chem. 265*, 2740−2748.

(10) Thillet, J., Adams, J. A., and Benkovic, S. J. (1990) The kinetic mechanism of wild-type and mutant mouse dihydrofolate reductases. *Biochemistry 29*, 5195−5202.

(11) Andrews, J., Fierke, C. A., Birdsall, B., Ostler, G., Feeney, J., Roberts, G. C. K., and Benkovic, S. J. (1989) A kinetic study of wild-type and mutant dihydrofolate reductases from *Lactobacillus casei*. *Biochemistry 28*, 5743−5750.

(12) Margosiak, S. A., Appleman, J. R., Santi, D. V., and Blakley, R. L. (1993) Dihydrofolate reductase from the pathogenic fungus *Pneumocystis carinii*: Catalytic properties and interaction with antifolates. *Arch. Biochem. Biophys. 305*, 499−508.

(13) Liang, P. H., and Anderson, K. S. (1998) Kinetic reaction scheme for the dihydrofolate reductase domain of the bifunctional thymidylate synthase-dihydrofolate reductase from *Leishmania major*. *Biochemistry 37*, 12206−12212.

(14) Lee, J., Yennawar, N. H., Gam, J., and Benkovic, S. J. (2010) Kinetic and Structural Characterization of Dihydrofolate Reductase from *Streptococcus pneumoniae*. *Biochemistry 49*, 195−206.

(15) Argyrou, A., Vetting, M. W., Aladegbami, B., and Blanchard, J. S. (2006) *Mycobacterium tuberculosis* dihydrofolate reductase is a target for isoniazid. *Nat. Struct. Mol. Biol. 13*, 408−413.

(16) Pace, C. N., Vajdos, F., Fee, L., Grimsley, G., and Gray, T. (1995) How to measure and predict the molar absorption coefficient of a protein. *Protein Sci. 4*, 2411−2423.

(17) Morrison, J.F. (1969) Kinetics of the reversible inhibition of enzyme-catalysed reactions by tight-binding inhibitors. *Biochim. Biophys. Acta 185*, 269−286.

(18) Morrison, J. F., and Stone, S. R. (1988) Mechanism of the reaction catalyzed by dihydrofolate reductase from *Escherichia coli*: pH and deuterium isotope effects with NADPH as the variable substrate. *Biochemistry 27*, 5499−5506.

(19) Johnson, K. A. (1992) Transient state kinetic analysis of enzyme reaction pathways. *Enzymes 20*, 1−61.

(20) Hiromi, K. (1979) *Kinetics of Fast Enzyme Reactions: Theory and Practice*, Halsted Press, New York.

(21) Cleland, W. W., and Northrop, D. B. (1999) Energetics of substrate binding, catalysis, and product release. *Methods Enzymol. 308*, 3−27.

(22) Winzor, D.J., and Jackson, C. M. (2006) Interpretation of the temperature dependence of equilibrium and rate constants. *J. Mol. Recognit. 19*, 389−407.

(23) Johnson, K. A., Simpson, Z. B., and Blom, T. (2009) Global Kinetic Explorer: A new computer program for dynamic simulation and fitting of kinetic data. *Anal. Biochem. 387*, 20−29.

(24) Johnson, K. A., Simpson, Z. B., and Blom, T. (2009) FitSpace Explorer: An algorithm to evaluate multidimensional parameter space in fitting kinetic data. *Anal. Biochem. 387*, 30−41.

(25) Qi, F., Dash, R. K., Han, Y., and Beard, D. A. (2009) Generating rate equations for complex enzyme systems by a computer-assisted systematic method. *BMC Bioinf. 10*, 238.

(26) Stewart, W. J. (2009) *Probability, Markov Chains, Queues, and Simulation: The Mathematical Basis of Performance Modeling*, Princeton University Press, Princeton, NJ.

(27) Northrop, D. B. (1975) Steady-state analysis of kinetic isotope effects in enzymic reactions. *Biochemistry 14*, 2644−2651.

(28) Carey, F. A., and Sundberg, R. J. (2000) *Advanced Organic Chemistry, Part A: Structures and Mechanisms*, 4th ed., Kluwer Academic, New York.

(29) Johnson, K. A. (1992) Transient-state kinetic analysis of enzyme reaction pathways. *Enzymes 20*, 1−61.

(30) Gore, M. G., and Bottomley, S. P. (2000) Stopped-flow fluorescence spectroscopy. In *Spectrophotometry and spectrofluorimetry* (Gore, M. G., Ed.) p 368, Oxford University Press, New York.

(31) Cleland, W.W. (1982) The use of pH studies to determine chemical mechanisms of enzyme-catalyzed reactions. *Methods Enzymol. 87*, 390−405.

(32) Maglia, G., Javed, M. H., and Allemann, R. K. (2003) Hydride transfer during catalysis by dihydrofolate reductase from *Thermotoga maritima*. *Biochem. J. 374*, 529−535.

(33) Chock, P. B., and Gutfreund, H. (1988) Reexamination of the kinetics of the transfer of NADH between its complexes with glycerol-3-phosphate dehydrogenase and with lactate dehydrogenase. *Proc. Natl. Acad. Sci. U.S.A. 85*, 8870−8874.

(34) Fersht, A. (1999) *Structure and Mechanism in Protein Science*, W. H. Freeman and Co., New York.

(35) Bennett, B. D., Kimball, E. H., Gao, M., Osterhout, R., Dien, S. J. V., and Rabinowitz, J. D. (2009) Absolute metabolite concentrations and implied enzyme active site occupancy in *Escherichia coli*. *Nat. Chem. Biol. 5*, 593−599.

(36) Gopinathan, K. P., Sirsi, M., and Ramakrishnan, T. (1963) Nicotin-amide-adenine nucleotides of *Mycobacterium tuberculosis* H37Rv. *Biochem. J. 87*, 444−448.

(37) Nakano, T., Spencer, H. T., Appleman, J. R., and Blakley, R. L. (1994) Critical role of phenylalanine 34 of human dihydrofolate reductase in substrate and inhibitor binding and in catalysis. *Biochemistry 33*, 9945−9952.

(38) Cleland, W. W., and Northrop, D. B. (1999) Energetics of substrate binding, catalysis, and product release. *Methods Enzymol. 308*, 3−27.